



HAL
open science

Ptbp1 and Exosc9 knockdowns trigger skin stability defects through different pathways

Maud Noiret, Stéphanie Mottier, Gaele Angrand, Carole Gautier-Courteille, Hubert Lerivray, Justine Viet, Luc Paillard, Agnès Méreau, Serge Hardy, Yann Audic

► **To cite this version:**

Maud Noiret, Stéphanie Mottier, Gaele Angrand, Carole Gautier-Courteille, Hubert Lerivray, et al.. Ptbp1 and Exosc9 knockdowns trigger skin stability defects through different pathways. *Developmental Biology*, 2016, 409 (2), pp.489-501. 10.1016/j.ydbio.2015.11.002 . hal-01225487

HAL Id: hal-01225487

<https://univ-rennes.hal.science/hal-01225487>

Submitted on 25 Jan 2016

HAL is a multi-disciplinary open access archive for the deposit and dissemination of scientific research documents, whether they are published or not. The documents may come from teaching and research institutions in France or abroad, or from public or private research centers.

L'archive ouverte pluridisciplinaire **HAL**, est destinée au dépôt et à la diffusion de documents scientifiques de niveau recherche, publiés ou non, émanant des établissements d'enseignement et de recherche français ou étrangers, des laboratoires publics ou privés.

Ptbp1 and Exosc9 knockdowns trigger skin stability defects through different pathways

Maud Noiret, Stéphanie Mottier, Gaele Angrand, Carole Gautier-Courteille, Hubert Lerivray, Justine Viet, Luc Paillard, Agnes Mereau, Serge Hardy, Yann Audic.

CNRS, UMR 6290 Institut Génétique et Développement de Rennes, Université de Rennes 1, Rennes, France

Corresponding author: Yann Audic

yann.audic@univ-rennes1.fr

CNRS, UMR 6290-Institut de Génétique et Développement de Rennes

Faculté de médecine

Université de Rennes I

2, Avenue du Professeur Léon Bernard

35043 RENNES Cedex

FRANCE

Tel.: 33 (0)2 2323 4475

Fax: 33 (0)2 2323 4478

ABSTRACT

In humans, genetic diseases affecting skin integrity (genodermatoses) are generally caused by mutations in a small number of genes that encode structural components of the dermal-epidermal junctions. In this article, we first show that inactivation of both *exosc9*, which encodes a component of the RNA exosome, and *ptbp1*, which encodes an RNA-binding protein abundant in *Xenopus* embryonic skin, impairs embryonic *Xenopus* skin development, with the appearance of dorsal blisters along the anterior part of the fin. However, histological and electron microscopy analyses revealed that the two phenotypes are distinct. *Exosc9* morphants are characterized by an increase in the apical surface of the goblet cells, loss of adhesion between the sensorial and peridermal layers, and a decrease in the number of ciliated cells within the blisters. *Ptbp1* morphants are characterized by an altered goblet cell morphology. Gene expression profiling by deep RNA sequencing showed that the expression of epidermal and genodermatosis-related genes is also differentially affected in the two morphants, indicating that alterations in post-transcriptional regulations can lead to skin developmental defects through different routes. Therefore, the developing larval epidermis of *Xenopus* will prove to be a useful model for dissecting the post-transcriptional regulatory network involved in skin development and stability with significant implications for human diseases.

Keywords: RNA-binding proteins; genodermatosis; post-transcriptional regulations; epidermis.

INTRODUCTION

In humans, epithelial stability defects are of genetic (genodermatosis) or autoimmune origin. Epidermolysis bullosa and Ehlers-Danlos syndrome are genetic disorders caused by mutations in genes that encode proteins of the extracellular matrix, such as collagen (COL7A1, COL1A1), intracellular proteins like plectin, or membrane-bound proteins involved in cell-cell or cell-substrate junctions, like laminins and non-fibrillar collagens (Fine et al., 2014). Cutis laxa is another form of skin syndrome in which mutations in a dozen genes lead to defective development of elastic skin fibers, resulting in loose skin and progeria-like features (Urban and Davis, 2014). Autoimmune forms of skin stability defects occur through the production of autoantibodies that target dermal-epidermal junction components, such as Bullous Pemphigoid Antigen 1 (BPAG1), encoded by the Distonin gene (*DST*, (Sawamura et al., 1990)), or BPAG2, encoded by the collagen 17 A1 gene (*COL17A1*, Nishie, 2014). Some key genes are identified as being mutated and some autoantigens are known, but the phenotypic variability of these diseases suggests that modifier genes may affect phenotype penetrance or expressivity (Kern et al., 2009).

While seemingly different, amphibian skin and mammal skin share a number of similarities. In both classes, a bilayered epidermis found in early embryos develops into a multilayered epidermis, consisting of basal, spinous, granular and cornified cells that are hierarchically-related and derived from the stem cells located in the basal layer. This hierarchical differentiation is thought to have emerged with amphibians about 350

million years ago. The embryonic bilayered epidermis is composed of external peridermal cells with a different lineage from the internal basal cells. The particularity of amphibians is that these basal cells initially differentiate into ciliated cells, ionocytes and small secretory cells to form a mucociliary epithelium upon intercalation into the external layer, which is composed of peridermal goblet cells. By 15 days of embryogenesis in mice and at metamorphosis in *Xenopus*, the bilayered epidermis is progressively replaced by a multilayered cornified epidermis that originates from the basal layer cells. Both larval and adult epidermis can be derived *in vitro* from larval basal cells. Therefore, larval basal cells are the direct precursors of adult epidermal stem cells (Suzuki et al., 2002; Yoshizato, 2007).

The *Xenopus* larval epidermis has historically been used as a model for analyzing cellular differentiation (Billett and Gould, 1971; Steinman, 1968). This epidermis has gained renewed attention recently as an important model for studying the development of the mucociliary epithelium and cell-cell interactions (Dubaisi and Papalopulu, 2011). As some genodermatoses are known to affect both skin and upper airways lined with multiciliated cells (Fine et al., 2007), the developing *Xenopus* epidermis is an attractive model for addressing questions relating to both of these systems. In this specific study, we use larval *Xenopus* skin to investigate the impact of post-transcriptional regulation on skin stability.

Through our previous work on *ptbp1*, we have shown that post-transcriptional regulations are required to control the developing epidermis (Le Sommer et al., 2005). The polypyrimidine track binding protein 1 (Ptbp1) is a conserved RNA-binding protein involved in the regulation of alternative splicing and polyadenylation, mRNA stability, localization and translation (Cote et al., 1999; Gosert et al., 2000; Hamon et al., 2004; Sawicka et al., 2008; Tillmar and Welsh, 2002). Thereby, Ptbp1 controls the abundance and identity of the protein expressed from the RNA to which it is bound. While Ptbp1 expression can be detected in many tissues, we have described a high expression in the epidermis of the developing *X. tropicalis* embryo (Noiret et al., 2012) and we have previously shown that its inactivation in *X. laevis* leads to alterations in the skin structure, with the formation of blisters in the dorsal fin epidermis (Le Sommer et al., 2005).

The exosome component 9 (Exosc9) is one of the core components of the RNA exosome, a conserved high-molecular-weight complex that is involved in RNA processing and degradation. The exosome has roles both in the nuclear and cytoplasmic compartments. In the nucleus, it is involved in primary transcript processing and the degradation of unprocessed or intergenic transcripts. In the cytoplasm, it plays a role in mRNA degradation through the 3-5' decay pathway (Garneau et al., 2007), controlling the turnover of mRNAs, for example those containing AU-rich elements found in cytokines and involved in the mRNA surveillance mechanism. It was recently shown that exosome components are enriched in epidermal progenitor cells (Mistry et al., 2012). This prompted us to test whether the exosome could play a role in skin differentiation using the *Xenopus* embryonic epidermis as a model system. In this paper, we report that the inactivation of Exosc9 by injection of antisense morpholino-oligonucleotides in *X. laevis* leads to the development of blister structures on the antero-dorsal part of the embryo that are similar to the structures observed in *ptbp1* morphants.

To determine whether Exosc9 and Ptbp1 share a common pathway in specifying the blister phenotype, we

conducted a comparative analysis of *exosc9* and *ptbp1* morphant embryos. We compared the phenotypes of the morphant embryos by histological analysis on sections, and analyzed the nature of the external epithelial cells using scanning electron microscopy (SEM). To address the phenotypic variations, we finally performed a differential analysis of gene expression in embryos depleted of *Ptbp1* or *Exosc9* using deep RNA sequencing. We conclude that epidermis defects in *exosc9* and *ptbp1* morphants differ significantly, and we discuss the implications of these findings for human pathology.

RESULTS

***Exosc9* knockdown causes dorsal fin defects**

To address the potential developmental function of *Exosc9*, we designed a translation inhibitory morpholino oligonucleotide targeting *exosc9* mRNA (Mo*Exosc9*). As no antibodies directed against *Xenopus Exosc9* were available, we controlled morpholino efficiency by injection of a reporter mRNA encoding a V5-tagged version of *Exosc9* (*Exosc9*-V5). Co-injection of Mo*Exosc9* with the *Exosc9*-V5 RNA led to a twofold decrease in the accumulation of the V5-tagged protein (**Figure 1A, compare lanes 1 and 2**). When a morpholino-resistant version of the tagged *exosc9* RNA was co-injected with the Mo*Exosc9*, no decrease in the V5-tagged protein was observed (**Figure 1A, lanes 3 and 4**). This illustrates that Mo*Exosc9* specifically blocks *exosc9* mRNA translation.

At stage 33, embryos depleted in *Exosc9* display several defects, including improper development of the epidermis with the appearance of blister structures along the anterior part of the dorsal fin (**Figure 1B**). These blister structures first appeared around stage 28 as ripples along the fin (data not shown) and were completely formed by stage 33 (**Figure 1B**). The embryos died by late tadpole stage. At stage 33, more than 80% of the injected embryos developed at least one dorsal blister (**Figure 1C**), indicating a strong penetrance of the phenotype. Embryos injected with the control morpholino (MoCo) did not present blisters (**Figure 1B**). The co-injection of *Exosc9*-V5R mRNA immune to the morpholino strongly reduced both blister number and volume (**Figure 1B, right panel**). These results show that *Exosc9* has a role to play in the formation of the dorsal fin epidermis and is probably required for proper skin development and stability.

Characterization of exosc9 and ptbp1 morphant embryos

A blister phenotype was also previously described in embryos depleted of *Ptbp1* by injection of a specific morpholino (Mo*Ptbp1*) (Le Sommer et al., 2005). We compared the blister phenotype of *ptbp1* and *exosc9* morphant embryos using a combination of *in situ* hybridization, histological sections and scanning electron microscopy.

To determine whether differentiation of the epithelial cells was altered, we first performed *in situ* hybridization with epithelial cells markers on albinos *X. laevis* embryos depleted in *Exosc9* or *Ptbp1* (**Figure 2**). We used the previously reported probes (see material and methods for details) *tuba1a*, *foxa1*, *foxi1* and *itln2* for detecting respectively: ciliated cells (cc, **Figure 2A-C**), small secretory cells (ssc, **Figure 2D-F**), ionocytes (I, **Figure 2G-I**) and goblet cells (gc, **Figure 2J-L**). We did not observe a striking difference in the number or

spatial distribution of any of these cell types between MoCo and MoExosc9- or MoPtbp1-injected embryos. Notably, the dorsal blisters were strongly labeled with *itln2*, showing that they are mostly composed of goblet cells (**Figure 2J-L**). However, some *tuba1a*, *foxi1* and *foxa1* positive cells were also present, indicating that the blisters are composed of goblet cells intermingled with ciliated cells, ionocytes and ssc. Therefore, no overall changes could be detected in the differentiation program of the sensorial layer or the periderm in any of the conditions.

Next, we performed a histological analysis of 5 μ m sections across the blisters of stage 40 embryos to analyze the structure of the blisters in more detail and determine whether the blisters were alike in MoExosc9- and MoPtbp1-injected embryos. Non-injected embryos (NI), *ptbp1* morphants and two *exosc9* morphants presenting different phenotypic severities (**Figure 3A**) are shown in **Figure 3 (B-Q)**. As previously described (Dubaisi and Papalopulu, 2011), the developing epidermis (ep) of control embryos is bilayered, comprising an internal layer of sensorial cells (slc, **Figure 3C-E**), overlaid by an outer epithelial layer that consists of four different cell types. The ciliated cells (cc) were easily identified morphologically by the presence of thin cilia on the pictures (**Figure 3C-D**), and pigment granules (pg) could be observed as brownish spots in the outer epithelial cell layer (**Figure 3D-E**). The dorsal fin blisters of both *exosc9* and *ptbp1* morphants were composed of a thin single cell layer (**Figure 3, compare panels G, K, O with panel C**). The dorsal blisters of *exosc9* morphants appeared to have fewer ciliated cells, defined by the presence of countable cilia (**Figure 3 K and O**). To further quantify this phenotype, we counted cilia positive cells along the dorsal blisters of the morphants (**Figure 3R**). The proportion of ciliated cells decreased about twofold ($p=0,01573$, t-test) between the MoExosc9 and non-injected embryos. No difference was observed between the MoPtbp1 and non-injected embryos. Outside of the blisters, the *ptbp1* morphant displayed a double layered epidermis with pigment granules (**Figure 3 H-I**). This was also the case of one of the *exosc9* morphants (**Figure 3L-M**), but, in some others, as shown for the *exosc9* embryo2 morphant, the blisters and lateral and ventral epidermis were composed of a single cell layer (**Figure 3 O-Q**). Therefore, while the *ptbp1* morphant phenotype is restricted to the dorsal side, the *exosc9* morphant phenotype can extend down to the ventral side. A striking feature in the *exosc9* embryo1 morphant was the gap between the sensorial cell layer and the epithelial cell layer (**Figure 3, panels J, L, M**) in which the sensorial cell layer appeared to be loose and slightly detached from the outer cell layer (**Figure 3, panels L, M; arrowhead**). This suggests that the adhesion between these two cell layers was altered. This gap is not observed in the *ptbp1* morphant (**Figure 3F-I**).

Together, these data show that, while *exosc9* and *ptbp1* morphants share a morphologically similar phenotype with a common monolayered epidermis in the blisters, they are histologically different. Indeed, *exosc9* morphants display a specific decrease in cells harboring cilia in the dorsal fin epidermis and a lack of adhesion between the sensorial and outer cell layer. This suggests that different processes come into play to disrupt the development of the epidermis in both morphants.

Exosc9 and ptbp1 morphants display distinct epidermal defects

Finally, we studied the organization of the outer epidermal layer by scanning electron microscopy. This technology is used to analyze and identify the different cell types located in the outer epidermal cell layer. They can also be identified by *in situ* hybridization (see **Figure 2**) or immunohistochemistry (Dubaissi et al., 2014). In addition, SEM enables a detailed analysis of cellular surface morphology. Our analysis focused on the lateral midbody of the embryos outside of the blister structures. At stage 26, three types of cells could be distinguished in the control embryos (**Figure 4 A, B**). Ciliated cells (cc) are characterized by the presence of large filamentous cilia, goblet cells (gc) — the initial and major components of the periderm — are observed as large mucus-secreting cells with small apical vacuoles and secretory granules, and ionocytes (i) are viewed as medium-sized cells with a smooth apical surface. By stage 36, an additional cell type intercalates into the outer layer of the epidermis. These small secretory cells (ssc) have recently been described (Dubaissi et al., 2014) and are observed as small triangular-shaped cells with large apical vacuoles (**Figure 4 C, D**). To detect any differences that may occur during skin differentiation, we analyzed the *exosc9* and *ptbp1* morphant embryos at stages 26 and 36. By stage 26, all three cell types (cc, gc, i) were present (**Figure 4**) in the *exosc9* and *ptbp1* morphants. While they appeared to be morphologically normal in the *exosc9* morphants (**Figure 4 I, J**), in *ptbp1* morphants the goblet cells were altered with a domed apical surface and a high density of secretion granules (**Figure 4 E, F**). By stage 36, the *ptbp1* morphant phenotype was reinforced with a swollen apical surface of the goblet cells and many secretory granules. Small secretory cells were now present and appeared unaffected (**Figure 4 G, H**). At stage 36, *exosc9* morphants displayed ssc and ionocytes that were morphologically unaffected, whereas the ciliated cells presented a reduction in the number of cilia, and the goblet cells appeared larger compared with the control embryos (**Figure 4 K, L**). To confirm this last observation, we quantified the goblet cell area in the control embryos and *ptbp1* and *exosc9* morphants at stage 36. Goblet cells were significantly larger in the *exosc9* morphants ($p < 5,02 \cdot 10^{-26}$, t-test) compared with the control embryos and their size was unaffected in the *ptbp1* morphants (**Figure 4M**).

We concluded from this analysis that the epidermis differed externally from the control in both the *ptbp1* and *exosc9* morphants but in different ways. While the goblet cells were the most morphologically affected cell type in *ptbp1* morphant embryos with a swollen apical surface and an increase in secretion vacuoles, in *exosc9* morphants, the ciliated cells were morphologically altered with a perturbed ciliogenesis and the goblet cells were larger than in the control embryos.

Transcriptome analysis of exosc9 and ptbp1 morphant embryos

Histological and scanning electron microscopy analysis of the outer layer of the epidermis showed that the *exosc9* and *ptbp1* morphant phenotypes were dissimilar. As *in situ* hybridization for markers of the four different cell types making up the epidermis did not show an obvious alteration in the differentiation of these cell types, *Ptbp1* or *Exosc9* depletion probably does not lead to a general disruption of the epidermal differentiation program (**Figure 2**). Therefore, to address the molecular basis of the phenotypes in more

detail and determine to what extent the transcriptome changes overlap in *ptbp1* and *exosc9* morphants, we carried out deep sequencing on the RNA extracted from stage 26 embryos when the blister phenotype is first evident. Two lines of argument indicated that Ptbp1 and Exosc9 were depleted by injection of the corresponding morpholinos in these particular experiments. Firstly, both the efficiency of MoPtbp1 and MoExosc9 has been demonstrated (Le Sommer et al. 2005 and **Figure 1A**). Secondly, in addition to collecting stage 26 embryos for RNA extraction, we allowed some siblings to develop until stage 36 for phenotypic analysis. About 90% of the *exosc9* and *ptbp1* morphant siblings generated for the RNAseq experiments had at least one blister consistent with the high penetrance of the phenotype (**Figure 5A**). We built unstranded sequencing libraries from stage 26 embryos, which were sequenced as 2x101 paired-end reads. About 85% of the reads could be unambiguously mapped to the 7.1 X. *laevis* genome with 75% of concordant pairs aligned (**Figure 5B**). Only concordant read pairs (aligned on the same scaffold in opposite directions) were kept for further analysis. To illustrate the nature of the results obtained from mapping reads to the *Xenopus* genome, we show a Sashimi plot (Wang et al., 2008) of the reads mapped to the *hmcn1* locus (one of the most overexpressed genes in both morphants, see below) in **Figure 5C**. The exon-intron structure of the gene was obvious from the mapped reads and could be compared with the annotation shown at the bottom. The relative abundance of reads mapped to the *hmcn1* locus was indicative of a higher expression of *hmcn1* in both *exosc9* and *ptbp1* morphants when compared with the control embryos.

To determine which genes are differentially expressed upon Ptbp1 or Exosc9 knockdown, we used a counting strategy in which the number of reads overlapping exons was totaled for each gene. Differential expression analysis was performed with DESEQ2 on a model using a binomial negative distribution (Love et al., 2014). Principal component analysis of log-transformed expression data showed that the replicates of each biological sample were clustered, and each of the experimental conditions could clearly be distinguished from the others (**Figure 5D**).

We identified the genes that were differentially expressed upon *ptbp1* (n=160) or *exosc9* (n=1258) knockdown (**Supplementary table 1, MoPtbp1 and MoExosc9**). *Ptbp1* was unaffected in MoExosc9-injected embryos and, reciprocally, *exosc9* was unchanged in MoPtbp1-injected embryos. Therefore, this rules out any direct control of *ptbp1* upon *exosc9* and conversely. It is noteworthy that *ptbp2* was strongly upregulated among genes differentially expressed in *ptbp1* morphant embryos. This is consistent with the PTBP regulatory feed-back loop demonstrated in human cells (Spellman et al., 2007) and *Xenopus* embryos (Méreau et al., 2015).

Unexpectedly, given the similar external phenotypes of *ptbp1* and *exosc9* morphants, only 29 genes were differentially expressed in both morphants (**Figure 5E**). The fold changes had the same sign in both morphants for 23/29 genes and the gene expression fold change in *exosc9* morphants was significantly correlated with that in *ptbp1* morphants (Spearman correlation coefficient $\rho=0.62$, $p=5 \cdot 10^{-4}$, **Figure 5F**). Hemicentin 1 (*hmcn1*), for which we present a Sashimi plot, is one of the most upregulated genes in both morphants. It encodes a protein localized in the extracellular matrix of epithelial cells and is involved in the response to mechanical stress. Since the commonly differentially regulated genes are few in number, they may correspond to an indirect signature of epidermal disorganization rather than hypothetical common

triggers of blister appearance.

Dissimilarities of Ptbp1 and Exosc9 post-transcriptional networks in epidermis biology

To determine whether similar pathways are altered in *exosc9* and *ptbp1* morphant embryos, we conducted a GO term enrichment analysis (**Figure 6A**, complete list in **Supplementary table 2**). Upon depletion of Ptbp1, we observed an enrichment in misregulated genes that encode intracellular components involved in maintaining cell integrity, such as the cortical cytoskeleton, stress fibers and the platelet dense tubular network. None of these terms was enriched in *exosc9* morphants. Upon Exosc9 depletion, the enrichment was evident for interface components between the cell and the extracellular space (“extracellular space”, “brush border membrane”, “proteinaceous extracellular membrane”). Only one GO term (“extracellular vesicular exosome”) was significantly enriched in both morphants. However, while 32 and 138 genes belonging to the extracellular vesicular exosome were differentially expressed in *ptbp1* and *exosc9* morphants, respectively, only six of these genes were shared by both morphants (*angptl2*, *arf1*, *fam162a*, *gsto1*, *gstp1*, *hmcn1*, *mgam*). Therefore, depletion of Ptbp1 and Exosc9 proteins has different consequences on cell components. Along with histological analysis, this gene enrichment analysis showed that the cells are affected differently by Ptbp1 and Exosc9 depletion.

To confirm these findings, we focused on a subset of genes relevant to epidermal biology. We first selected 58 genes specifically expressed in the epidermis, based on previous publications (Chalmers et al., 2006; Hayes et al., 2007), and assessed how their expression levels were affected in *ptbp1* and *exosc9* morphants (**Supplementary table 3**). **Figure 6B** revealed slightly greater dynamic changes in RNA levels in *exosc9* morphants ($\log_2(\text{FoldChange})$ (LFC) ranging from -1.07 to 2.93) compared with *ptbp1* morphants (LFC ranging from -0.84 to 1.57). The epidermal gene expression fold changes in *exosc9* morphants were poorly correlated with those in *ptbp1* morphants (Spearman correlation coefficient $\rho=0.34$, $p=0.03$, **Figure 6B**). Indeed, a number of markers were significantly affected in only one of the two morphants (for example *grhl3* or *eppk1*, which are respectively upregulated and downregulated in *exosc9* morphants, but unchanged in *ptbp1* morphants) or had opposite behaviors (like *atp6v1a*). Together, these findings demonstrate that *exosc9* and *ptbp1* knockdowns have distinct consequences on epidermal gene expression.

We next assessed how well these gene expression data matched previous phenotype characterization (**Figures 2-4**). The SEM data (**Figure 4**) revealed intense morphological perturbations of the goblet cells in *ptbp1* morphants. This was not the case in *exosc9* morphants, despite an increased surface area. Accordingly, two goblet cell markers — *itln2* and *mapk12* — were altered in opposite directions in *ptbp1* morphants and were unaffected in *exosc9* morphants (**Figure 6B**). This suggests that inactivation of Ptbp1 remodels gene expression in the goblet cells. The SEM data also showed altered ciliogenesis in *exosc9* but not in *ptbp1* morphants. It was therefore interesting to observe that the ciliated cell markers *tuba1a*, *ttc25* and *tubb6* were downregulated in *exosc9* but not in *ptbp1* morphants (**Figure 6B**).

To determine whether this downregulation of ciliary genes could be generalized, we compared the

distribution of ciliary gene fold changes (SYSCILIA database, (van Dam et al., 2013) between the *exosc9* and *ptbp1* morphants overall. In **Figure 6C**, we present the cumulative distribution function [cdf: $y=(\text{fraction of genes with a log fold-change} \leq x)$ plotted against x] of the fold change quantified in *exosc9* and *ptbp1* morphants. The *exosc9* morphant distribution was shifted to the left of the *ptbp1* morphant distribution (shoulder highlighted by the arrow). For example, 10% of ciliary genes in *exosc9* morphants had a $\log_2(\text{FC})$ below -0.5, but this only concerned 1.5% of ciliary genes in *ptbp1* morphants. This indicates that, overall, the repression of ciliary genes in *exosc9* morphants was stronger than in *ptbp1* morphants. The gene expression analysis is therefore fully consistent with the phenotypic analysis of *ptbp1* and *exosc9* morphants.

Genodermatosis genes are differentially misexpressed between *exosc9* and *ptbp1* morphants

To investigate the relevance of our findings for human pathologies, we analyzed the *Xenopus* orthologs of genes known to be mutated in several genodermatoses, such as Epidermolysis bullosa (Fine et al., 2014), Ehlers-Danlos syndrome (Byers and Murray, 2014), Kindler syndrome (Jobard et al., 2003; Siegel et al., 2003), acral peeling skin syndrome (Cassidy et al., 2005) and Naxos disease (McKoy et al., 2000). These gene products are involved in hemidesmosomes, desmosomes or adherens junction (plakoglobin) and focal adhesion, as depicted in **Figure 7B**. **Figure 7A** and **Supplementary Table 4** show the expression of genodermatosis genes in *ptbp1* and *exosc9* morphants. The genodermatosis genes that are differentially expressed in *ptbp1* morphants are involved in Ehler-Danlos syndrome (*col1a1*, *col1a2*) or Kindler syndrome (*femr1*). The genodermatosis genes that are differentially expressed in *exosc9* morphants are involved in acral peeling skin syndrome (*tgm5*) or Naxos disease (*jup*). Finally, genes causal in Epidermolysis bullosa were found both within the differentially expressed genes in *ptbp1* morphants (*dst*) and the differentially expressed genes in *exosc9* morphants (*krt5*, *lama3*, *dsp*, *plec*, *itga6*). *Col17a1*, also involved in Epidermolysis bullosa, was differentially expressed in both morphants but was upregulated in *exosc9* morphants and downregulated in *ptbp1* morphants. Together, these data show that depletions of Ptbp1 and Exosc9 induce different types of skin stability defects.

We also investigated how these gene products were distributed between the different subcellular structures involved in cell adhesion (**Figure 7B**). Focal adhesions and the extracellular matrix contain proteins encoded by genes that are differentially expressed in *ptbp1* morphants. Desmosomes contain proteins encoded by genes that are differentially expressed in *exosc9* morphants, and hemidesmosomes contain proteins encoded by genes that are differentially expressed in both morphants. Mutations in any one of these genes can cause human skin stability syndromes (Cassidy et al., 2005; Fine et al., 2014). It is therefore highly probable that the concomitant dysregulation of several of these genes is resulting in the appearance of the *ptbp1* or *exosc9* morphant phenotypes.

In conclusion, we demonstrated that both *exosc9* and *ptbp1* morphant embryos specifically develop skin instability defects that could be clearly distinguished both histologically and at transcriptome level. This demonstrates that Exosc9 and Ptbp1 act through different regulatory pathways to control larval skin stability.

DISCUSSION

In this article, we showed that specific inactivation of *Ptbp1* and *Exosc9*, which encode two proteins involved in RNA metabolism, leads to skin stability defects in *Xenopus laevis* embryos. At first glance, the macroscopic phenotypes of both *exosc9* and *ptbp1* morphants are similar, with the appearance of blisters along the dorsal fin of the embryos. This phenotype is associated with normal early epidermal differentiation, as deduced from the expression of markers for all cell types in the epidermis.

While the normal epidermis is composed of two cell layers, blisters are composed of a single layer of cells in both morphants. Histology, SEM and gene profiling analysis show that the morphant phenotypes differ in several ways: the apparent adhesion properties of the outer cell layer, the identity of the most strongly affected cells (ciliated cells in *exosc9* morphants, goblet cells in *ptbp1* morphants), the nature of the misexpressed genes (both taken overall and focusing on epidermal markers, ciliary genes or genodermatosis genes), and the enriched GO pathways. We therefore conclude that both *Ptbp1* and *Exosc9* contribute to skin stability, but through different routes.

The *Ptbp1* route includes the downregulation of several components of the dermal-epidermal junction, such as *col1a1*, *col1a2*, *col17a1* or *BPAG2 (dst)*. Mutations in the human *COL1A1* and *COL1A2* genes have been directly implicated in Ehlers-Danlos syndrome, a condition that results in alteration of skin elasticity. In *X. laevis*, *col1a1* expression is initially limited to the dorsal epidermal layers of the embryo (Goto et al., 2000; Grimaldi et al., 2004), suggesting that the dorsal localization of the blisters could be due, in part, to the downregulation of *col1a1* in *ptbp1* morphants. The *COL17A1* protein (BPAG180) is a hemidesmosome component which is targeted by autoantibodies in bullous pemphigoid (Sawamura et al., 1990). The *COL17A1* gene is also mutated in some benign forms of junctional Epidermolysis bullosa (Bauer and Lanschuetzer, 2003).

While the constitutive knockout of *Ptbp1* is lethal in early mouse development (Shibayama et al., 2009; Suckale et al., 2011), the conditional inactivation of *Ptbp1* in the mouse telencephalon leads to disruption of the ciliated epithelial layer lining the inside of the brain ventricles (Shibasaki et al., 2013). While the *PTBP1* targets responsible for this phenotype remain unknown, the loss of epithelial integrity is correlated with a mislocalization of adherens junction components. Correct development of adherens junctions is known to enable the correct formation of other cell-cell junctions, such as desmosomes (Lai-Cheong et al., 2007; Todorovic et al., 2014). Our model for early inactivation of *ptbp1* in *Xenopus* provides a unique and easily accessible means of addressing the role of *ptbp1* in cell-cell or cell-substrate junction formation.

Interestingly, we recently described a regulatory feedback loop in which the epithelial-specific splicing regulator *Esrp1* positively and specifically controls *Ptbp1* abundance in the epidermis (Méreau et al., 2015). Knockdown of *Esrp1* expression leads to a blister phenotype that correlates with decreased *Ptbp1* expression in the skin of *esrp1* morphants. By investigating to what extent the *Esrp1* phenotype recapitulates the *Ptbp1* phenotype, we should get a new insight into the post-transcriptional regulatory network at play during larval skin development.

The Exosc9 route is characterized by the upregulation of *krt5*, *tgm5*, *lama3* and *jup*, and the downregulation of *itga6*, *plec* and *dsp*. Mutations in these four genes are causal in human Epidermolysis bullosa (*KRT5*, *LAMA3*, *ITGA6*, *PLEC*, *DSP*), acral peeling syndrome (*TGM5*) and Naxos disease (*JUP*). The *exosc9* morphant phenotype is accompanied by changes in the relative expression of four structural genes linking epithelial cells to the basement membrane (*krt5*, *lama3*, *itga6*, *plec*, see **Figure 7B**). These changes may contribute to skin instability and the development of blisters. More specifically, two desmosomal components that are inversely affected, *jup* and *dsp*, may be involved in the loss of adhesion observed between the sensorial cells and the outer cell layer in the *exosc9* morphants. The epiplakin (*eppk1*) and grainy-head like 3 transcription factor (*grhl3*) genes also deserve particular attention. *Eppk1* is repressed in *exosc9* morphants and is a marker of the superficial cells of the epidermis (Chalmers et al., 2006). Identification of EPPK1 as an autoantigen in a patient suffering from a blistering disease (Fujiwara et al., 1996) would point towards a possible causal relationship between the downregulation of *eppk1* and the appearance of blisters in *exosc9* morphants. However, the absence of obvious skin defects in *Eppk1*^{-/-} mice renders this hypothesis less likely (Spazierer et al., 2006). Mutations in the *GRHL3* gene lead to Van der Woude syndrome, including abnormal oral periderm development (Peyrard-Janvid et al., 2014). Furthermore, the overexpression of *grhl3* upon inactivation of Exosc9 is consistent with the observation that EXOSC9 triggers the degradation of *Grhl3* mRNA in human epidermal stem cells. Upon differentiation of the epidermal stem cells, Exosc9 activity decreases, allowing the accumulation of *Grhl3* mRNA and turning on its specific expression program (Mistry et al., 2012). In this model, knockdown of *Exosc9* by siRNA led to the overexpression of *Grhl3* mRNA, resulting in a decrease in cell proliferation, an increase in cell differentiation and a reduced number of cells in the basal layer. Upon *exosc9* knockdown in *Xenopus*, we observed an alteration of the sensorial cell layer with the appearance of gaps between the inner and outer cell layer or the development of a monolayered epidermis. As cells located in the sensorial cell layer act as progenitor cells to generate the cell type diversity observed in the epithelial layer, it is possible that Exosc9 plays a similar function in the developing embryo. In *Xenopus*, early overexpression of *grhl3* in the whole embryo leads to a thickening of the deep epidermal cell layer accompanied, at stage 14, by an overexpression of superficial markers (Chalmers et al., 2006). We do not observe any thickening of the epidermis in *exosc9* morphants. This difference may be accounted for by a localized overexpression of *grhl3* after inactivation of *exosc9* in the embryo, as opposed to the overall and early expression after injection of mRNAs encoding Grhl3.

Here we uncover a link between Ptbp1, Exosc9 and skin stability, which, for the first time, provides evidence in a model organism that alterations in post-transcriptional regulatory networks can cause skin instability. These results draw attention to the molecular causes for skin defects in *ptbp1* and *exosc9* morphants. At first glance, this issue could be addressed by screening candidate genes found to be misexpressed in *ptbp1* or *exosc9* morphants to identify those whose knockdown phenocopies MoPtbp1- or MoExosc9-injection. Indeed, morpholino-mediated knockdown of *col17a1* or *cola1* in zebrafish (Durán et al., 2011; Kim et al., 2010), or *fermt1* (kindlin) in *Xenopus* (Rozario et al., 2014) results in skin instability. More generally, several animal models of genodermatoses have been produced (Bruckner-Tuderman et al., 2010), which generally phenocopy the disease by targeting genes that encode key structural components of the dermal-epidermal

complex. Yet, the expression of most genes is only mildly affected in *ptbp1* or *exosc9* morphants (generally by no more than a twofold factor at mRNA level, see **Figures 6B or 7A**). A modification of this magnitude of one gene alone may not be sufficient to trigger skin instability. Therefore, we favor the hypothesis that it is the concomitant dysregulation of several unidentified genes that explains the *ptbp1* and *exosc9* morphant phenotypes.

The *ptbp1* and *exosc9* morphant phenotypes are reminiscent of skin stability defects observed in human genodermatoses, which draws attention to the relevance of our findings for human disease. Skin stability defects in humans often occur through mutations or functional inactivation of genes that encode structural proteins of the dermal-epidermal complex, or through the development of autoantibodies against these proteins. However, the variability of clinical symptoms in patients suggests that “modifier” genes can modulate the expressivity of the disease. The nature of these modifier genes remains largely unknown. They can be specific alleles of components of the dermal-epidermal complex, as was demonstrated recently for *Col17a1* in the context of *Lamc2* mutation in mice (Sproule et al., 2014), but genes directly affecting the gene expression program may also be involved. Among them, our results identify *EXOSC9* and *PTBP1* as strong candidates for modifier genes involved in human skin instability syndromes. In addition, the orthologs of the genes found to be dysregulated and which are directly controlled by *Ptbp1* and *Exosc9* are also good candidates for modifier genes.

They can be identified by integrating RNASeq data with data from the immunoprecipitation of RNA/protein complexes and sequencing of the bound RNAs. With the ongoing advances in *Xenopus* genome annotation and the Crispr/CAS9 system (Harrison et al., 2014), *Xenopus* will be an invaluable model for examining the effects of the identified genes responding to post-transcriptional regulators in establishing and maintaining the stability of the developing epidermis.

MATERIALS AND METHODS

Plasmids, oligonucleotides and in vitro transcription

The coding sequence for Exosc9 was amplified from the Image clone (IRBHp990G0531D) with Exosc9_fwd (GGGGATCCATGAGTCTATAGTTATATGA) and Exosc9_rev (GGGCGGCCGCCTTTTGTGCAGATTTATTCTT) for the wild-type construct and Exosc9_res (GGGGATCCACCATGAACTCCGCTGTCCAACACTGT) and Exosc9_rev for the rescue plasmid. The PCR products were cloned into pGEM-T-easy (Promega) then digested with *Bam*HI and *Not*I and subcloned into pT7TSV5 (Hamon et al., 2004), digested with *Bgl*III and *Not*I beforehand. All constructs were verified by sequencing. The transcription templates were linearized using *Bam*HI. *In vitro* transcriptions were carried out using the T7 mMessage Machine (Ambion) according to manufacturer recommendations to produce the Exosc9_V5 and Exosc9_V5Rescue mRNAs. The antisense morpholino oligonucleotides were purchased from Gene-Tools (MoPtpb1 and MoCo see (Le Sommer et al., 2005), MoExosc9 (CGTCTCCTTCATGTCTGTAACACAC).

Xenopus embryos and microinjection

Xenopus laevis eggs were obtained from WT or albino females and fertilized using standard procedures (Paris et al., 1988). When indicated, 25 ng of MoExosc9, 30 ng of MoPtpb1 or 30 ng of control morpholino (GeneTools) was injected into each blastomere of two-cell embryos in a volume of 13.8 nl, using a Nanoject II (Drummond). For rescue experiments, 1 fmol of mRNA-encoding morpholino-resistant Exosc9-V5R was co-injected. Embryos were allowed to develop at 22°C and collected according to Nieuwkoop and Faber stages (Nieuwkoop and Faber, 1994). Anti-V5 (Life technologies) and anti-PCNA (Sigma-Aldrich) antibodies were diluted 1/5000. The polyclonal anti-Ptpb1 antibody was used at 1/500, as previously described (Hamon et al., 2004). To detect the primary antibodies, secondary antibodies coupled to alkaline phosphatase were used (Jackson laboratories). Phosphatase activity was detected by ECF (Amersham Biosciences) and quantified on a Storm 840 (Molecular Dynamics).

In situ hybridization

Plasmids containing cDNA for *tuba1a* (NM001086587), *foxA1* (BI445589, IMAGE:4680765), *itln2* (XL020e14) and *foxi1* (BC042303, IMAGE:4682602) were linearized and used as templates for *in vitro* transcription as follows: *tuba1a*, antisense probe, *Not*I, T7; sense probe, *Apal*, T3. *foxA1*, antisense probe, *Sall*, T7; sense probe *Not*I, SP6. *itln2*, antisense probe, *Eco*RI, T7; sense probe, *Xho*I, T3. *foxi1*, antisense probe, *Sall*, T7; sense probe, *Sph*I, SP6. Digoxigenin (Roche)-labeled antisense and sense probes were generated by *in vitro* transcription using the above-mentioned RNA polymerases (Promega). Whole-mount *in situ* hybridization was performed, as previously described (Harland, 1991), using an automated system (Intavis InsituPro VSi). Detection was carried out using anti-DIG Alkaline Phosphatase-conjugated antibodies

(Roche) and stained with NBT/BCIP (Promega) as a substrate. Images were taken on a Leica MZ165 with a DFC290HD camera.

RNAseq analysis

Total RNA was extracted using RNeasy columns (Qiagen) from a pool of 10 embryos at stage 26, previously injected with 25 ng of MoExosc9 or 30 ng of MoPtpb1 in both blastomeres of two-cell embryos.

Contaminating DNA was removed using TurboDnase (Ambion) and RNA quality was confirmed on a Bioanalyzer 2100 using an RNA Pico 6000 chip (Agilent). RNA was quantified by spectrometry on a Nanodrop ND-1000. Polyadenylated mRNAs were selected and unstranded libraries were prepared from 1 µg of total RNA using the TruSeq RNA sample low-throughput kit (Illumina) according to manufacturer recommendations. Thirteen PCR cycles were required to generate enough library material for sequencing. The libraries were quantified using the Qubit fluorimeter with the dsDNA BR kit (Invitrogen). Library size distribution was controlled on a Bioanalyzer 2100 using the DNA1000 chips (Agilent). Sequencing was performed on a HiSeq 2000 (Illumina) as 2x101 paired-end data. Reads were submitted to the European Nucleotide Archive (PRJEB8711). After sequencing and demultiplexing, read quality was controlled using FASTQC (<http://www.bioinformatics.babraham.ac.uk/projects/fastqc>). Reads were mapped to the *Xenopus laevis* 7.1 genome (available from Xenbase) using Tophat2 (Kim et al., 2013), allowing up to two matches for each read to take the pseudo-tetraploidy of the species into account (Pollet and Mazabraud, 2006). We determined the differentially expressed genes in MoPtpb1 and MoExosc9 by comparing the mapped reads with non-injected embryos, using DESEQ2 (v1.8.1) and the JGlv15 annotation available from Xenbase (Bowes et al., 2010). We considered the genes with a Benjamini-Hochberg adjusted p-value below 0.05 (BH-adjusted pvalue <0.05) as differentially expressed. Non-injected control embryos were used because the transcriptomic consequence of a control morpholino was likely to be dependent on the sequence of the control morpholino used and would later impair comparison with other forms of functional inactivation. Gene Ontology enrichment analysis was conducted based on the human orthologs of the *Xenopus* genes (HCOP). Statistical analysis was conducted with R using the topGO package (Alexa et al., 2006).

Scanning electron microscopy and histology

For scanning electron microscopy, embryos were fixed in MEMFA, dehydrated in methanol and processed for critical point dehydration, and coated and imaged on a JEOL JSM 6301F. For histological analysis, embryos were fixed in Bouin's solution (Sigma-Aldrich), dehydrated in ethanol, included in paraplast (McCormick Scientific) and processed for 5 µm transversal sections with a microtome (Leica). Sections were mounted, stained with hematoxylin/eosin and scanned (Nanozoomer NDP, Hamamtsu).

ACKNOWLEDGMENTS

The authors would like to thank the members of the many laboratories that contributed to the genomic data and annotations that have been made available to the community through Xenbase. Many thanks to Michelle Ware from the IGDR for correcting the English. The authors acknowledge the contribution of the University of Rennes I's CMEBA for the scanning electron microscopy, and the contribution of the Biosit (UMS CNRS 3480/US INSERM 018) H2P2 platform for the *in situ* hybridization experiments. Library sequencing was made possible by funding from the GENOSCOPE (AP10/11-DP15) and Maud Noiret was funded by a Ph.D fellowship from the French Ministry of National Education, Higher Education and Research.

LEGENDS

Figure 1: Exosc9 morphant embryos specifically display dorsal skin blisters

A) We injected two-cell embryos with the indicated molecules: morpholino targeting *exosc9* mRNA (MoExosc9), mRNA encoding a V5-tagged Exosc9 (Exosc9-V5) and mRNA mutated on the morpholino recognition site encoding a V5-tagged Exosc9 (Exosc9-V5R). We allowed the embryos to develop until stage 26 to assess the accumulation of V5-tagged protein by western blot. PcnA is the loading control. B) Photographs of stage 33 embryos previously injected with the indicated molecules. Arrows point to blisters. C) The blister phenotype was scored according to the number of dorsal blisters. The number of embryos scored for each experimental condition is indicated under the graph.

Figure 2: *In situ* hybridization for epidermal markers in *exosc9* and *ptbp1* morphants

Albino embryos were injected with the control morpholino (MoCo, A, D, G, J), MoPtbp1 (B, E, H, K) or MoExosc9 (C, F, I, L) in both blastomeres. Embryos were fixed at stage 32 and processed for *in situ* hybridization with the following probes: *tuba1a* (A-C), *foxa1* (D-F), *foxi1* (G-I) and *itln2* (J-L).

Figure 3: Histological comparison of *ptbp1* and *exosc9* morphant embryos

Embryos were injected with MoPtbp1 or MoExosc9 in both blastomeres, fixed at stage 40 and processed for histological analysis. A) Macroscopically, *ptbp1* and *exosc9* morphant embryos displayed similar blister structures on the dorsal side. B-Q) 5 μ m transversal sections from the embryos presented in A (section plans shown by white line) and stained with hematoxylin/eosin. Detailed images of the dorsal fin (C, G, K, O), and the lateral (D, H, L, P) and ventral (E, I, M, Q) epidermis were shown for each embryo as indicated. Abbreviations: epidermis (ep), neural tube (nt), notochord (nc), somite (sm), sensorial layer cells (slc), ciliated cells (cc) and pigment granule (pg). The scale bar is shown for each image (100 μ m, except B, F, J, N 1 mm). Arrowhead points to gap between slc and periderm layer. R) Cells harboring cilia were counted in the dorsal epithelium and normalized to the number of nuclei observed. The number of embryos and sections counted is presented below each barplot.

Figure 4: Scanning Electron Microscopy (SEM) analysis of the peridermal layer of *ptbp1* and *exosc9* morphant embryos

A-L) Stage 26 (A, B, E, F, I, J) and stage 36 (C, D, G, H, K, L) embryos, previously injected with MoPtbp1 or MoExosc9 or left uninjected (control) as indicated, were fixed, dehydrated and processed for SEM. The four cell types described in the *Xenopus* mucociliary epithelium are indicated as ionocytes (i), goblet cells (gc), ciliated cells (cc) and small secretory cells (ssc). **M)** The apical area of the goblet cells was measured in stage 36 embryos (MoCo 262 cells, 4 embryos; MoPtbp1 131 cells, 3 embryos; MoExosc9 168 cells, 4 embryos). The scale bar shown on pictures represents 10 μm (A, C, E, G, I, K) or 100 μm (B, D, F, H, J, L). Abbreviations: dorsal fin (df), eye (e), blister (bl).

Figure 5: Transcriptome analysis

A) Scoring of the blister phenotypes obtained in stage 36 embryos, the siblings of those used to prepare the RNA sequencing libraries. The number of scored embryos is indicated below the categories. B) Unstranded poly(A)⁺ RNA sequencing libraries were prepared from biological triplicates of pools of 10 embryos either non-injected (NI), or injected with MoPtbp1 or MoExosc9. Sequencing generated 2 x 10¹ nt paired reads. The total number of reads obtained (InputReads), the percentage of reads aligned (Overall_read_aligned) and of concordant pairs of reads aligned for each sample is indicated. C) Example of a Sashimi plot representing read coverage across the *hmcn1* locus in the three experimental conditions (samples 1). D) Principal component analysis of the nine samples discriminates between the experimental conditions. E) Venn diagram showing the overlap between differentially expressed genes (BH-adjusted pvalue <0.05 and at least twofold fold changes) in *ptbp1* and *exosc9* morphants. F) Log₂ fold changes (LFC) are presented for genes differentially expressed in *ptbp1* and *exosc9* morphant embryos.

Figure 6: Post-transcriptional networks of Ptbp1 and Exosc9 in epidermis biology

A) Comparison of enriched GO terms in differentially expressed genes in *ptbp1* and *exosc9* morphants. The dotted red line indicates p=0.05. B) Comparison of the fold change in *exosc9* (MoExosc9_Log₂(FC)) and *ptbp1* (MoPtbp1_Log₂(FC)) morphant embryos for genes encoding epidermal markers (Chalmers et al., 2006; Hayes et al., 2007). Genes significantly (p <0.05 corrected for multiple testing) differentially expressed in *ptbp1* morphants are shown in red, those significantly differentially expressed in *exosc9* morphants are shown in green and those significantly differentially expressed in both morphants are shown in black. C) Cumulative distribution of the Log₂ fold-change of ciliary genes following Exosc9 depletion (green) and Ptbp1 depletion (red), compared with the non-injected embryos. Differential expression of ciliary genes in *exosc9* and *ptbp1* morphant embryos.

Figure 7: Differential expression of genodermatosis-causing genes

A) Comparison of the fold changes in *exosc9* (MoExosc9_Log2(FC)) and *ptbp1* (MoPtpb1_Log2(FC)) morphant embryos for genes causing genodermatosis in humans. B) Schematic diagram of the dermal-epidermal junction in relation to genes differentially expressed upon Ptpb1 or Exosc9 depletion. Genes significantly ($p < 0.05$ corrected for multiple testing) differentially expressed in *ptbp1* morphants are highlighted with a red dot, those significantly differentially expressed in *exosc9* morphants with a green dot and those significantly differentially expressed in both morphants with a black dot. Abbreviations: HD, hemidesmosome; FA, focal adhesion; DES, desmosome.

HIGHLIGHTS

- *Exosc9* and *ptbp1* knockdown triggers blister development in the dorsal *Xenopus* epidermis
- Multiciliated cell development is compromised in *Exosc9* morphants
- Embryos depleted in Ptpb1 and Exosc9 display phenotypically different skin defects
- Ptpb1 and Exosc9 differentially control expression of genodermatosis-related genes

REFERENCES

- Alexa, A., Rahnenführer, J., and Lengauer, T. (2006). Improved scoring of functional groups from gene expression data by decorrelating GO graph structure. *Bioinformatics* 22, 1600–1607.
- Bauer, J.W., and Lanschuetzer, C. (2003). Type XVII collagen gene mutations in junctional epidermolysis bullosa and prospects for gene therapy. *Clin. Exp. Dermatol.* 28, 53–60.
- Billett, F.S., and Gould, R.P. (1971). Fine structural changes in the differentiating epidermis of *Xenopus laevis* embryos. *J. Anat.* 108, 465–480.
- Bowes, J.B., Snyder, K.A., Segerdell, E., Jarabek, C.J., Azam, K., Zorn, A.M., and Vize, P.D. (2010). Xenbase: gene expression and improved integration. *Nucleic Acids Res.* 38, D607–D612.
- Bruckner-Tuderman, L., McGrath, J.A., Robinson, E.C., and Uitto, J. (2010). Animal models of epidermolysis bullosa: update 2010. *J. Invest. Dermatol.* 130, 1485–1488.
- Byers, P.H., and Murray, M.L. (2014). Ehlers–Danlos syndrome: A showcase of conditions that lead to understanding matrix biology. *Matrix Biology* 33, 10–15.
- Cassidy, A.J., van Steensel, M.A.M., Steijlen, P.M., van Geel, M., van der Velden, J., Morley, S.M., Terrinoni, A., Melino, G., Candi, E., and McLean, W.H.I. (2005). A homozygous missense mutation in TGM5 abolishes epidermal transglutaminase 5 activity and causes acral peeling skin syndrome. *Am. J. Hum. Genet.* 77, 909–917.
- Chalmers, A.D., Lachani, K., Shin, Y., Sherwood, V., Cho, K.W.Y., and Papalopulu, N. (2006). Grainyhead-like 3, a transcription factor identified in a microarray screen, promotes the specification of the superficial layer of the embryonic epidermis. *Mech. Dev.* 123, 702–718.
- Cote, C.A., Gautreau, D., Denegre, J.M., Kress, T.L., Terry, N.A., and Mowry, K.L. (1999). A *Xenopus* protein related to hnRNP I has a role in cytoplasmic RNA localization. *Mol. Cell* 4, 431–437.
- van Dam, T.J., Whewey, G., Slaats, G.G., SYSCILIA Study Group, Huynen, M.A., and Giles, R.H. (2013). The SYSCILIA gold standard (SCGSv1) of known ciliary components and its applications within a systems biology consortium. *Cilia* 2, 7.
- Dubaissi, E., and Papalopulu, N. (2011). Embryonic frog epidermis: a model for the study of cell-cell interactions in the development of mucociliary disease. *Dis Model Mech* 4, 179–192.
- Dubaissi, E., Rousseau, K., Lea, R., Soto, X., Nardeosingh, S., Schweickert, A., Amaya, E., Thornton, D.J., and Papalopulu, N. (2014). A secretory cell type develops alongside multiciliated cells, ionocytes and goblet cells, and provides a protective, anti-infective function in the frog embryonic mucociliary epidermis. *Development* 141, 1514–1525.
- Durán, I., Marí-Beffa, M., Santamaría, J.A., Becerra, J., and Santos-Ruiz, L. (2011). Actinotrichia collagens and their role in fin formation. *Dev. Biol.* 354, 160–172.
- Fine, J.-D., Johnson, L.B., Weiner, M., and Suchindran, C. (2007). Tracheolaryngeal complications of inherited epidermolysis bullosa: cumulative experience of the national epidermolysis bullosa registry. *Laryngoscope* 117, 1652–1660.
- Fine, J.-D., Bruckner-Tuderman, L., Eady, R.A.J., Bauer, E.A., Bauer, J.W., Has, C., Heagerty, A., Hintner, H., Hovnanian, A., Jonkman, M.F., et al. (2014). Inherited epidermolysis bullosa: updated recommendations on diagnosis and classification. *J. Am. Acad. Dermatol.* 70, 1103–1126.

- Fujiwara, S., Kohno, K., Iwamatsu, A., Naito, I., and Shinkai, H. (1996). Identification of a 450-kDa Human Epidermal Autoantigen as a New Member of the Plectin Family. *J Invest Dermatol* 106, 1125–1130.
- Garneau, N.L., Wilusz, J., and Wilusz, C.J. (2007). The highways and byways of mRNA decay. *Nat Rev Mol Cell Biol* 8, 113–126.
- Gosert, R., Chang, K.H., Rijnbrand, R., Yi, M., Sangar, D.V., and Lemon, S.M. (2000). Transient expression of cellular polypyrimidine-tract binding protein stimulates cap-independent translation directed by both picornaviral and flaviviral internal ribosome entry sites *In vivo*. *Mol. Cell. Biol.* 20, 1583–1595.
- Goto, T., Katada, T., Kinoshita, T., and Kubota, H.Y. (2000). Expression and characterization of *Xenopus* type I collagen alpha 1 (COL1A1) during embryonic development. *Dev. Growth Differ.* 42, 249–256.
- Grimaldi, A., Tettamanti, G., Martin, B.L., Gaffield, W., Pownall, M.E., and Hughes, S.M. (2004). Hedgehog regulation of superficial slow muscle fibres in *Xenopus* and the evolution of tetrapod trunk myogenesis. *Development* 131, 3249–3262.
- Hamon, S., Le Sommer, C., Mereau, A., Allo, M.-R., and Hardy, S. (2004). Polypyrimidine tract-binding protein is involved *in vivo* in repression of a composite internal/3' -terminal exon of the *Xenopus* alpha-tropomyosin Pre-mRNA. *J. Biol. Chem.* 279, 22166–22175.
- Harland, R.M. (1991). *In situ* hybridization: an improved whole-mount method for *Xenopus* embryos. *Methods Cell Biol.* 36, 685–695.
- Harrison, M.M., Jenkins, B.V., O'Connor-Giles, K.M., and Wildonger, J. (2014). A CRISPR view of development. *Genes Dev.* 28, 1859–1872.
- Hayes, J.M., Kim, S.K., Abitua, P.B., Park, T.J., Herrington, E.R., Kitayama, A., Grow, M.W., Ueno, N., and Wallingford, J.B. (2007). Identification of novel ciliogenesis factors using a new *in vivo* model for mucociliary epithelial development. *Dev. Biol.* 312, 115–130.
- Jobard, F., Bouadjar, B., Caux, F., Hadj-Rabia, S., Has, C., Matsuda, F., Weissenbach, J., Lathrop, M., Prud'homme, J.-F., and Fischer, J. (2003). Identification of mutations in a new gene encoding a FERM family protein with a plectstrin homology domain in Kindler syndrome. *Hum. Mol. Genet.* 12, 925–935.
- Kern, J.S., Grüninger, G., Imsak, R., Müller, M.L., Schumann, H., Kiritsi, D., Emmert, S., Borozdin, W., Kohlhase, J., Bruckner-Tuderman, L., et al. (2009). Forty-two novel COL7A1 mutations and the role of a frequent single nucleotide polymorphism in the MMP1 promoter in modulation of disease severity in a large European dystrophic epidermolysis bullosa cohort. *Br. J. Dermatol.* 161, 1089–1097.
- Kim, D., Pertea, G., Trapnell, C., Pimentel, H., Kelley, R., and Salzberg, S.L. (2013). TopHat2: accurate alignment of transcriptomes in the presence of insertions, deletions and gene fusions. *Genome Biol.* 14, R36.
- Kim, S.H., Choi, H.Y., So, J.-H., Kim, C.-H., Ho, S.-Y., Frank, M., Li, Q., and Uitto, J. (2010). Zebrafish type XVII collagen: gene structures, expression profiles, and morpholino “knock-down” phenotypes. *Matrix Biol.* 29, 629–637.
- Lai-Cheong, J.E., Arita, K., and McGrath, J.A. (2007). Genetic diseases of junctions. *J. Invest. Dermatol.* 127, 2713–2725.
- McKoy, G., Protonotarios, N., Crosby, A., Tsatsopoulou, A., Anastasakis, A., Coonar, A., Norman, M., Baboonian, C., Jeffery, S., and McKenna, W.J. (2000). Identification of a deletion in plakoglobin in arrhythmic right ventricular cardiomyopathy with palmoplantar keratoderma and woolly hair (Naxos disease). *Lancet* 355, 2119–2124.

Méreau, A., Anquetil, V., Lerivray, H., Viet, J., Schirmer, C., Audic, Y., Legagneux, V., Hardy, S., and Paillard, L. (2015). A posttranscriptional mechanism that controls Ptbp1 abundance in the *Xenopus* epidermis. *Mol. Cell. Biol.* 35, 758–768.

Mistry, D.S., Chen, Y., and Sen, G.L. (2012). Progenitor function in self-renewing human epidermis is maintained by the exosome. *Cell Stem Cell* 11, 127–135.

Nieuwkoop, P.D., and Faber, J. (1994). *Normal Table of *Xenopus Laevis* (Daudin): A Systematical and Chronological Survey of the Development from the Fertilized Egg Till the End of Metamorphosis* (Garland Pub.).

Nishie, W. (2014). Update on the pathogenesis of bullous pemphigoid: an autoantibody-mediated blistering disease targeting collagen XVII. *J. Dermatol. Sci.* 73, 179–186.

Noiret, M., Audic, Y., and Hardy, S. (2012). Expression analysis of the polypyrimidine tract binding protein (PTBP1) and its paralogs PTBP2 and PTBP3 during *Xenopus tropicalis* embryogenesis. *Int. J. Dev. Biol.* 56, 747–753.

Peyrard-Janvid, M., Leslie, E.J., Kousa, Y.A., Smith, T.L., Dunnwald, M., Magnusson, M., Lentz, B.A., Unneberg, P., Fransson, I., Koillinen, H.K., et al. (2014). Dominant Mutations in GRHL3 Cause Van der Woude Syndrome and Disrupt Oral Periderm Development. *The American Journal of Human Genetics* 94, 23–32.

Pollet, N., and Mazabraud, A. (2006). Insights from *Xenopus* genomes. *Genome Dyn* 2, 138–153.

Rozario, T., Mead, P.E., and DeSimone, D.W. (2014). Diverse functions of kindlin/fermitin proteins during embryonic development in *Xenopus laevis*. *Mech. Dev.* 133, 203–217.

Sawamura, D., Nomura, K., Sugita, Y., Mattei, M.G., Chu, M.L., Knowlton, R., and Uitto, J. (1990). Bullous pemphigoid antigen (BPAG1): cDNA cloning and mapping of the gene to the short arm of human chromosome 6. *Genomics* 8, 722–726.

Sawicka, K., Bushell, M., Spriggs, K.A., and Willis, A.E. (2008). Polypyrimidine-tract-binding protein: a multifunctional RNA-binding protein. *Biochem. Soc. Trans.* 36, 641–647.

Shibasaki, T., Tokunaga, A., Sakamoto, R., Sagara, H., Noguchi, S., Sasaoka, T., and Yoshida, N. (2013). PTB deficiency causes the loss of adherens junctions in the dorsal telencephalon and leads to lethal hydrocephalus. *Cereb. Cortex* 23, 1824–1835.

Shibayama, M., Ohno, S., Osaka, T., Sakamoto, R., Tokunaga, A., Nakatake, Y., Sato, M., and Yoshida, N. (2009). Polypyrimidine tract-binding protein is essential for early mouse development and embryonic stem cell proliferation. *FEBS J.* 276, 6658–6668.

Siegel, D.H., Ashton, G.H.S., Penagos, H.G., Lee, J.V., Feiler, H.S., Wilhelmsen, K.C., South, A.P., Smith, F.J.D., Prescott, A.R., Wessagowit, V., et al. (2003). Loss of kindlin-1, a human homolog of the *Caenorhabditis elegans* actin-extracellular-matrix linker protein UNC-112, causes Kindler syndrome. *Am. J. Hum. Genet.* 73, 174–187.

Le Sommer, C., Lesimple, M., Méreau, A., Menoret, S., Allo, M.-R., and Hardy, S. (2005). PTB regulates the processing of a 3'-terminal exon by repressing both splicing and polyadenylation. *Mol. Cell. Biol.* 25, 9595–9607.

Spazierer, D., Fuchs, P., Reipert, S., Fischer, I., Schmuth, M., Lassmann, H., and Wiche, G. (2006). Epiplakin Is Dispensable for Skin Barrier Function and for Integrity of Keratin Network Cytoarchitecture in Simple and Stratified Epithelia. *Mol. Cell. Biol.* 26, 559–568.

Spellman, R., Llorian, M., and Smith, C.W.J. (2007). Crossregulation and Functional Redundancy between the Splicing Regulator PTB and Its Paralog nPTB and ROD1. *Molecular Cell* 27, 420–434.

Sroufe, T.J., Bubier, J.A., Grandi, F.C., Sun, V.Z., Philip, V.M., McPhee, C.G., Adkins, E.B., Sundberg, J.P., and Roopenian, D.C. (2014). Molecular identification of collagen 17a1 as a major genetic modifier of laminin gamma 2 mutation-induced junctional epidermolysis bullosa in mice. *PLoS Genet.* 10, e1004068.

Steinman, R.M. (1968). An electron microscopic study of ciliogenesis in developing epidermis and trachea in the embryo of *Xenopus laevis*. *Am. J. Anat.* 122, 19–55.

Suckale, J., Wendling, O., Masjkur, J., Jäger, M., Münster, C., Anastassiadis, K., Stewart, A.F., and Solimena, M. (2011). PTBP1 is required for embryonic development before gastrulation. *PLoS ONE* 6, e16992.

Suzuki, K., Utoh, R., Kotani, K., Obara, M., and Yoshizato, K. (2002). Lineage of anuran epidermal basal cells and their differentiation potential in relation to metamorphic skin remodeling. *Dev. Growth Differ.* 44, 225–238.

Tillmar, L., and Welsh, N. (2002). Hypoxia may increase rat insulin mRNA levels by promoting binding of the polypyrimidine tract-binding protein (PTB) to the pyrimidine-rich insulin mRNA 3'-untranslated region. *Mol. Med.* 8, 263–272.

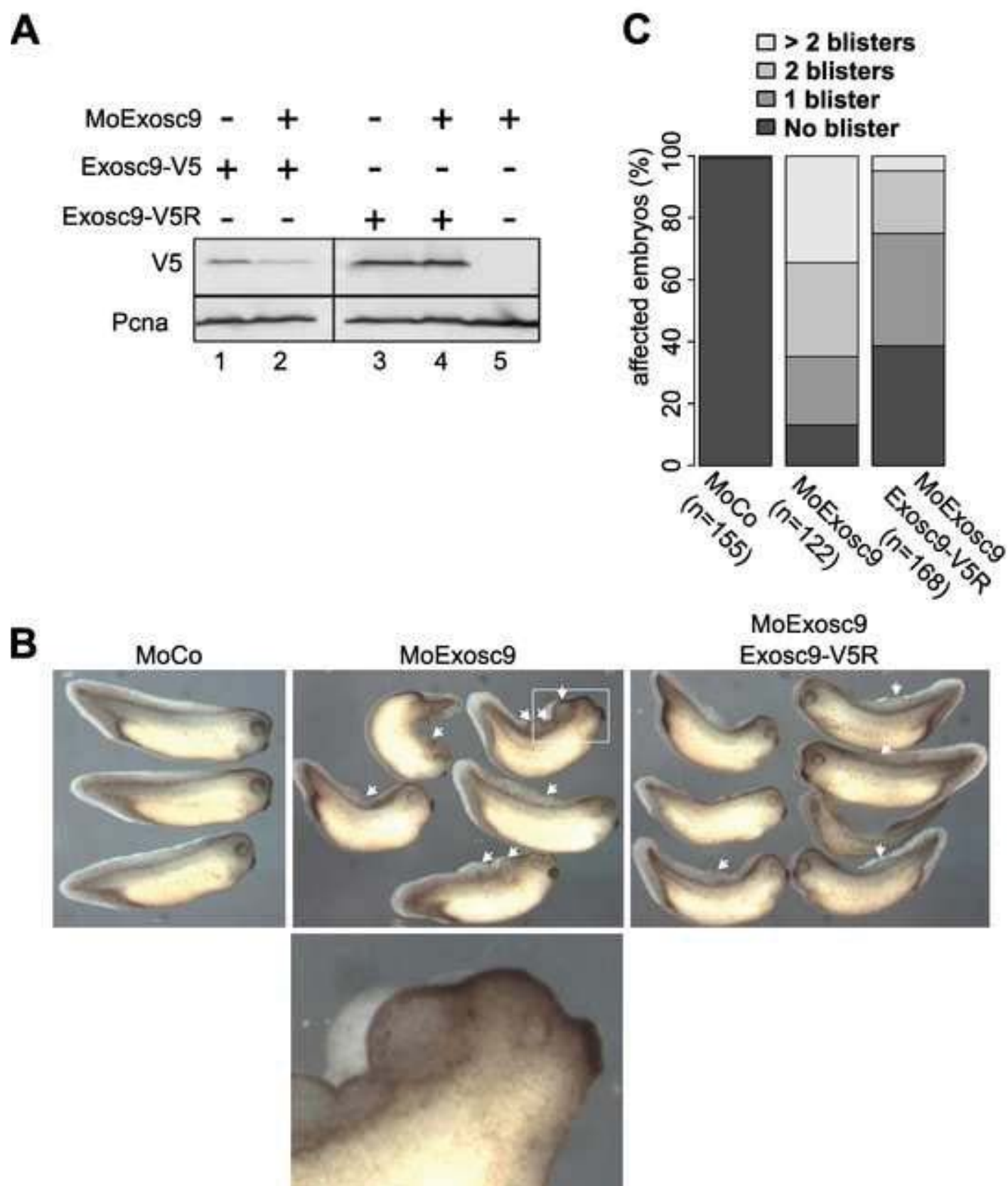
Todorovic, V., Koetsier, J.L., Godsel, L.M., and Green, K.J. (2014). Plakophilin 3 mediates Rap1-dependent desmosome assembly and adherens junction maturation. *Mol. Biol. Cell* 25, 3749–3764.

Urban, Z., and Davis, E.C. (2014). Cutis laxa: intersection of elastic fiber biogenesis, TGF β signaling, the secretory pathway and metabolism. *Matrix Biol.* 33, 16–22.

Yoshizato, K. (2007). Molecular mechanism and evolutionary significance of epithelial-mesenchymal interactions in the body- and tail-dependent metamorphic transformation of anuran larval skin. *Int. Rev. Cytol.* 260, 213–260.

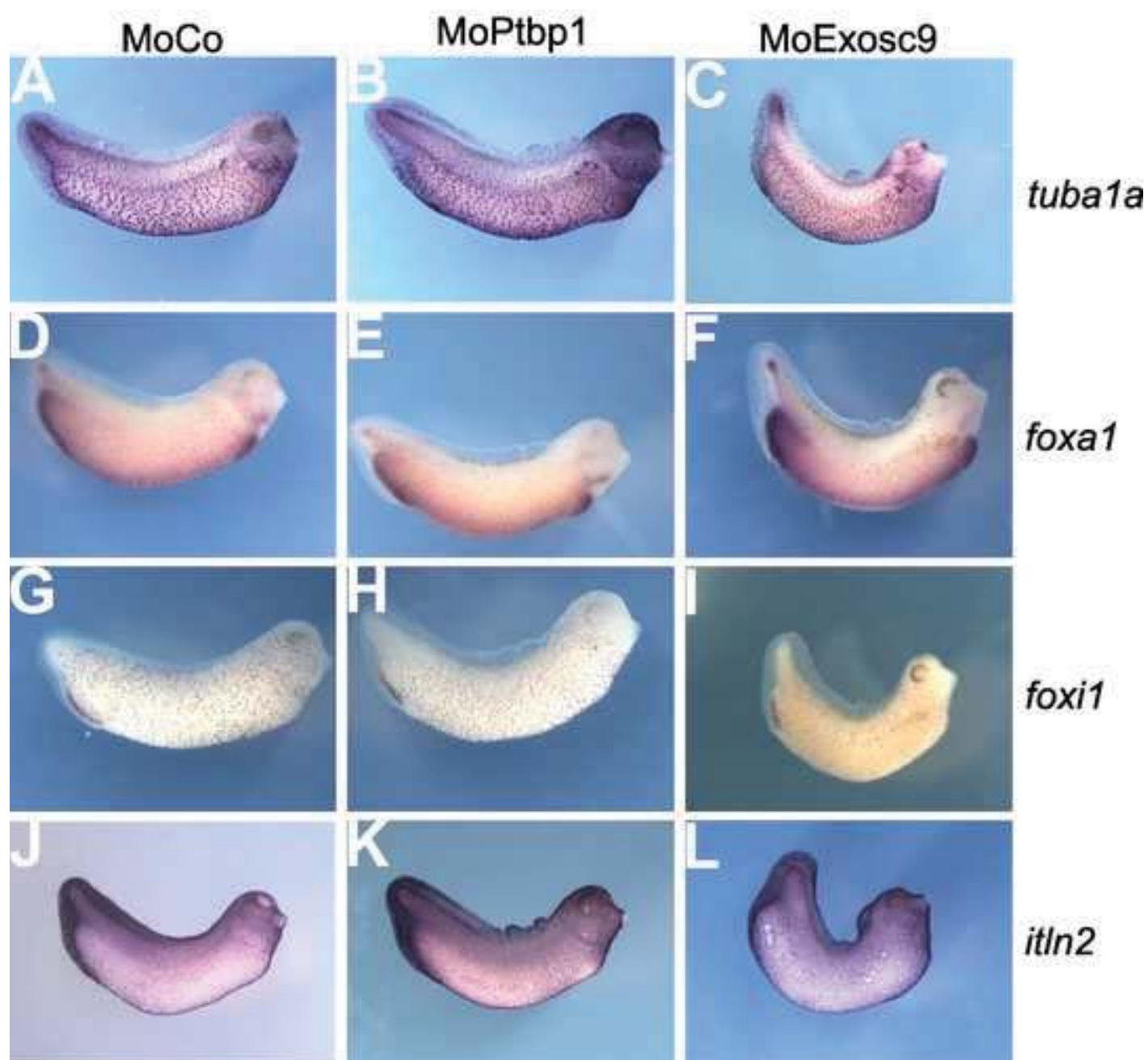
NOIRET_FIGURE 1

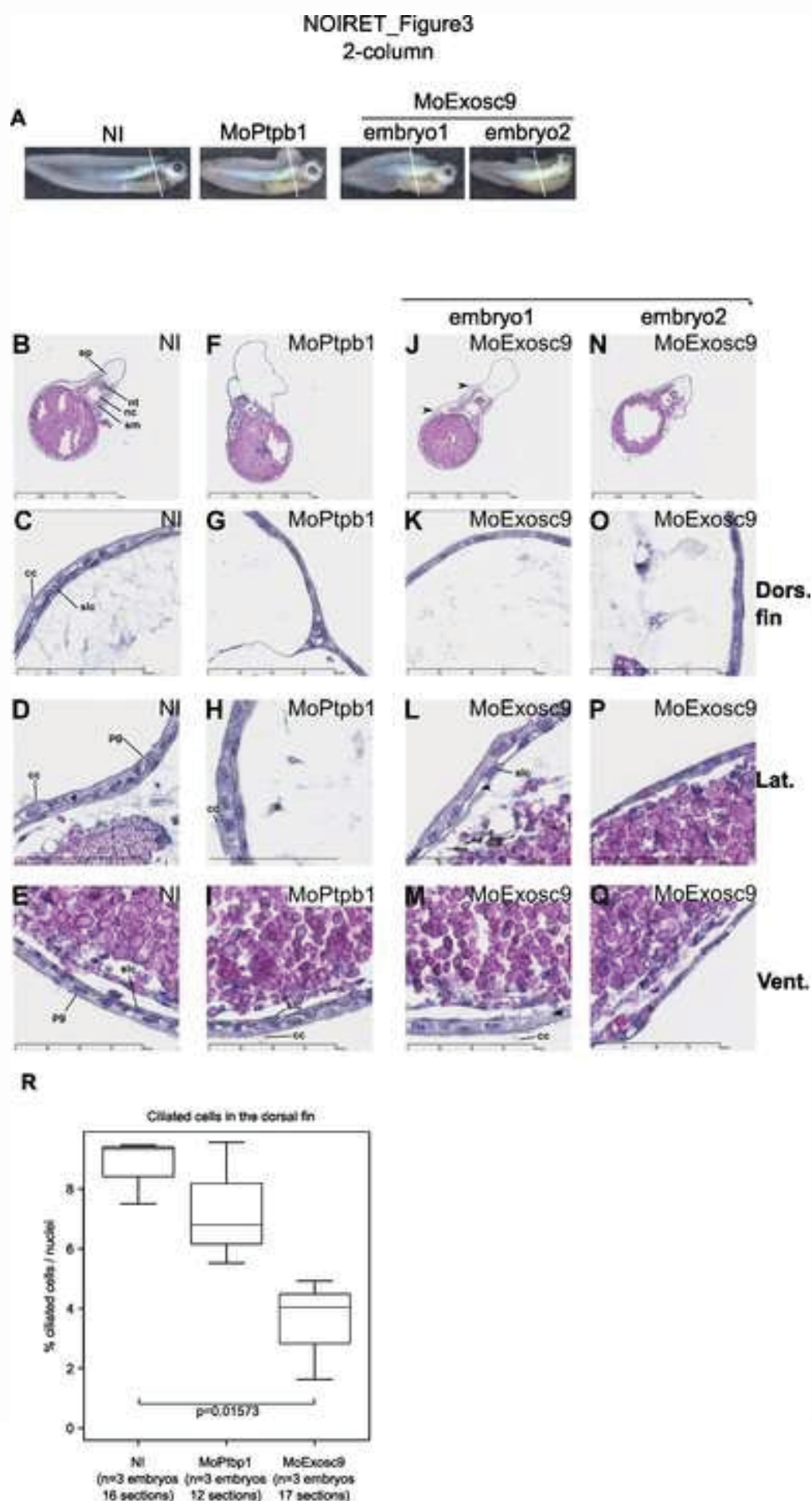
1.5 column

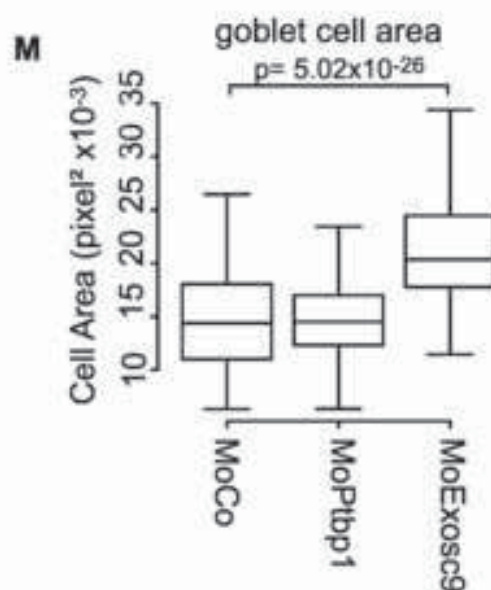
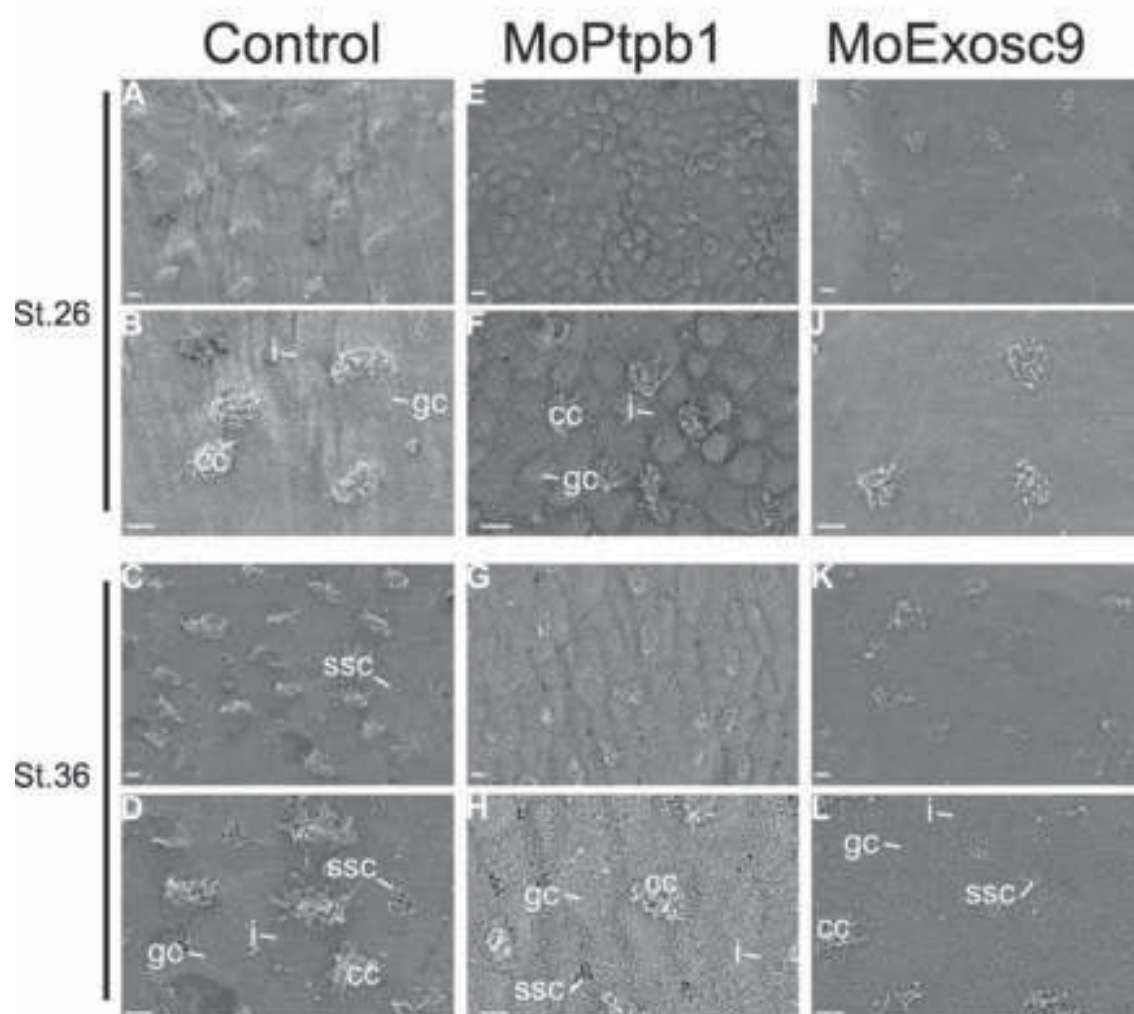


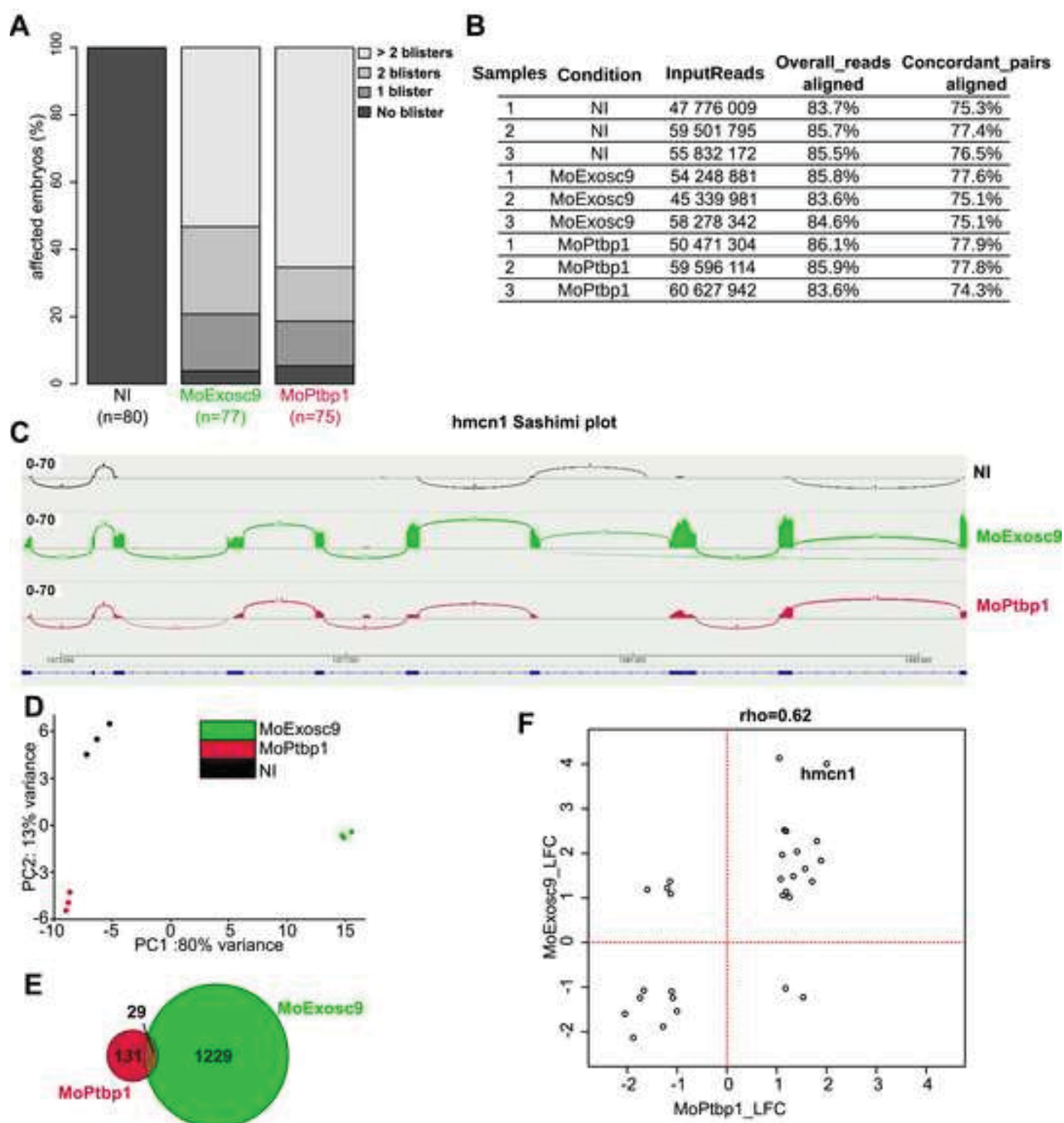
NOIRET_FIGURE 2

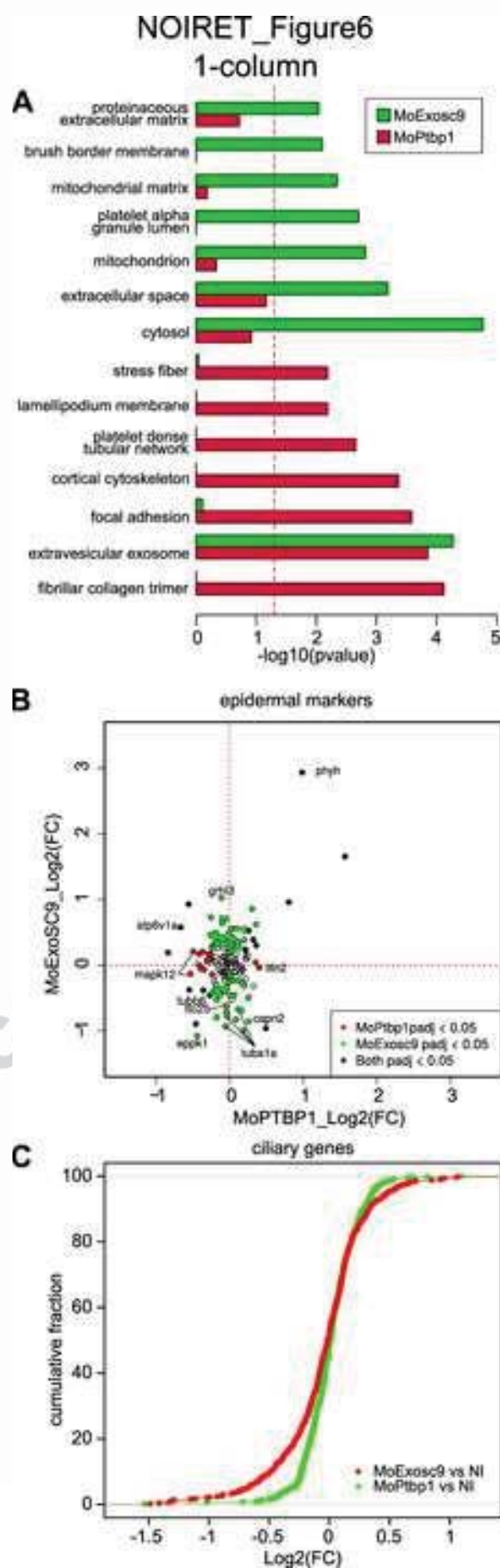
1.5 column





NOIRET_FIGURE4
2-column

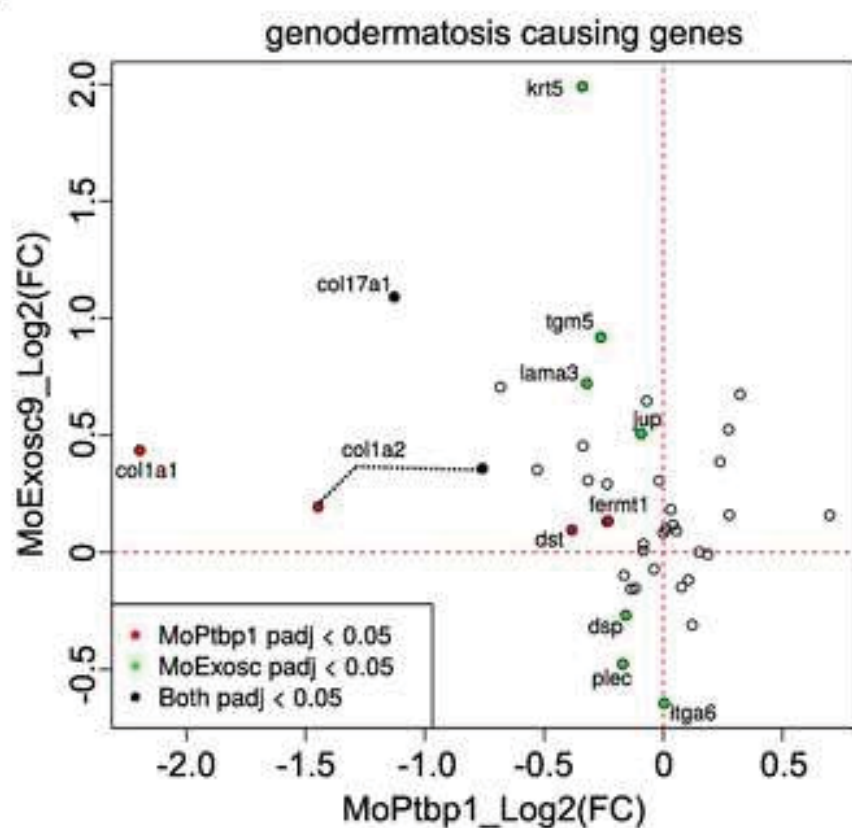
NOIRET_Figure5
2-column



NOIRET_Figure7

1-column

A



B

